Research article

NMR IN BIOMEDICINE

Received: 28 September 2012, Revised: 25 January 2013, Accepted: 14 February 2013, Published online in Wiley Online Library: 2 April 2013

(wileyonlinelibrary.com) DOI: 10.1002/nbm.2942

A calibration-based approach to real-time *in vivo* monitoring of pyruvate C_1 and C_2 polarization using the J_{CC} spectral asymmetry

Justin Y. C. Lau[a,b], Albert P. Chen[c], Yi-Ping Gu[b] and Charles H. Cunningham[a,b]*

A calibration-based technique for real-time measurement of pyruvate polarization by partial integral analysis of the doublet from the neighbouring *J*-coupled carbon is presented. *In vitro* calibration data relating the C_2 and C_1 asymmetries to the instantaneous C_1 and C_2 polarizations, respectively, were acquired in blood. The feasibility of using the *in vitro* calibration data to determine the instantaneous *in vivo* C_1 and C_2 polarizations was demonstrated in the analysis of rat kidney and pig heart spectral data. An approach for incorporating this technique into *in vivo* protocols is proposed. Copyright © 2013 John Wiley & Sons, Ltd.

Keywords: hyperpolarized; pyruvate; DNP; carbon-13; polarization measurement; asymmetry

INTRODUCTION

Dynamic nuclear polarization (DNP) is a non-equilibrium spin population technique that can provide a temporary, liquid-state ^{13}C NMR signal enhancement of more than four orders of magnitude (1). This signal enhancement facilitates rapid MR observation of ^{13}C *in vivo* (2). One application of particular interest is the *in vivo* monitoring of pyruvate metabolism, which has been shown to change with the onset of numerous disease conditions, including cancer (3) and cardiovascular diseases (4). Quantitative analysis of metabolism requires knowledge of the DNP signal enhancement at all time points such that the spectral intensity can be normalized to concentration, allowing for comparison within a series of measurements. Signal enhancement, or equivalently spin polarization, is conventionally determined by comparison with the corresponding thermal equilibrium signal intensity. Acquisition of a thermal equilibrium carbon spectrum *in vivo* is difficult due to the prohibitively long scan times required to obtain an adequate signal-to-noise ratio (SNR). An alternative approach to polarization measurement is needed for *in vivo* applications.

In measuring the polarization of [^{13}C] urea, Ardenkjaer-Larsen *et al*. examined the normalized difference of partial integrals for the two spectral lines in the ^{15}N doublet, which arise from *J*-coupling with the adjacent ^{13}C nucleus (1). This approach was extended to pyruvate using an analogous partial integrals analysis of the homonuclear *J*-coupled C_2 doublet to estimate the C_1 polarization of [1,2-$^{13}C_2$] pyruvate and [1-^{13}C] pyruvate (from 1% natural abundance of [1,2-$^{13}C_2$] pyruvate) in solution (5). Hurd *et al*. reported that, in solution at 3 T, the T_1 of the C_1 carbon in [1,2-$^{13}C_2$] pyruvate (56 s) was only slightly shorter than that in [1-^{13}C] pyruvate (60 s). The feasibility of measuring the C_1 polarization of [1-^{13}C] pyruvate using the relative spectral intensities of the C_2 doublet (1% natural abundance) has been demonstrated *in vitro* and *in vivo* (6). Although accurate for initial polarization measurement, the C_2 doublet was found to evolve beyond the second-order spectral pattern of a strongly *J*-coupled AB spin system at thermal equilibrium soon after injection of the pre-polarized solution into an animal. The physical mechanisms responsible for the evolution of C_2 doublet asymmetry in the [1,2-$^{13}C_2$] pyruvate system have not been fully understood.

The objective of this research is to extend the work of Hurd *et al*. and Chen *et al*. to enable the measurement of instantaneous C_1 polarization regardless of the time elapsed post-injection. After a brief examination of the theoretical framework underlying polarization measurements based on doublet partial integrals, we pursue an empirical approach. We use calibration data in blood that are consistent with our animal protocols to determine the instantaneous *in vivo* polarization in rat kidney and pig heart metabolic experiments.

* *Correspondence to: C. H. Cunningham, Imaging Research (M7-613), Sunnybrook Health Sciences Centre, 2075 Bayview Ave., Toronto, Ontario, Canada, M4N 3M5.*
E-mail chuck@sri.utoronto.ca

a *J. Y. C. Lau, C. H. Cunningham*
Department of Medical Biophysics, University of Toronto, Toronto, Ontario, Canada

b *J. Y. C. Lau, Y.-P. Gu, C. H. Cunningham*
Imaging Research, Sunnybrook Research Institute, Toronto, Ontario, Canada

c *A. P. Chen*
GE Healthcare, Toronto, Ontario, Canada

Abbreviations used: *DNP, dynamic nuclear polarization; SNR, signal-to-noise ratio; RF, radiofrequency; FA, flip angle; Gd-HP-DO3A, gadolinium (III) 2-[4-(2-hydroxypropyl)-7,10-bis(2-oxido-2-oxoethyl)-1,4,7,10-tetrazacyclododec-1-yl]acetate (gadoteridol); Tris, tris(hydroxymethyl)aminomethane; EDTA, ethylenediaminetetraacetic acid; Gd-DTPA, gadolinium (III) diethylenetriaminepentaacetic acid; RNU, Rowett nude; GEVPDF, generalized extreme value probability density function; Pyr, pyruvate (keto form); Pyh, pyruvate hydrate (gem-diol form); MCT1, monocarboxylate transporter 1.*

THEORY

The Hamiltonian operator representing a system of two *J*-coupled ^{13}C nuclei is given in Equation [1]. In the case of negligible *J*-coupling, $J_{CC} \approx 0$ Hz, there are four stationary states: $|\alpha\alpha\rangle$, $|\alpha\beta\rangle$, $|\beta\alpha\rangle$, and $|\beta\beta\rangle$, where the notation $|\psi_1\psi_2\rangle$ represents an ordered tensor product of the two nuclear spin wavefunctions $|\psi_1\rangle_{C_1} \otimes |\psi_2\rangle_{C_2}$. For non-zero J_{CC}, $|\alpha\alpha\rangle$ and $|\beta\beta\rangle$ remain eigenstates, but two new eigenstates arise from mixtures of $|\alpha\beta\rangle$ and $|\beta\alpha\rangle$, as summarized in Figure 1.

$$\hat{\mathcal{H}}_0 = \omega_1 \hat{I}_{z_1} + \omega_2 \hat{I}_{z_2} + 2\pi J_{CC} \hat{\mathbf{I}}_1 \cdot \hat{\mathbf{I}}_2 \qquad [1]$$

The C_1 polarization is the fractional occupation of levels where $|\psi_1\rangle_{C_1} = |\alpha\rangle$ less the fractional occupation of levels where $|\psi_1\rangle_{C_1} = |\beta\rangle$. From Figure 1, the desired C_1 polarization as a function of time $P_{C_1}(t)$ can be written as

$$P_{C_1}(t) = \frac{\left[N_1(t) + |c_2|^2 N_2(t) + |c_1|^2 N_3(t)\right] - \left[|c_1|^2 N_2(t) + |c_2|^2 N_3(t) + N_4(t)\right]}{N_1(t) + N_2(t) + N_3(t) + N_4(t)} \qquad [2]$$

For a single nucleus, the transition probability W_{ij} between two spin states $|\psi_i\rangle$ and $|\psi_j\rangle$ is given by Fermi's golden rule, Equation [3], where $\hat{\mathcal{H}}_1$ is the perturbative Hamiltonian operator, ρ is the density of final states, and the integration is performed over the solid angle Ω. The probability of transition in either direction is the same, $W_{i\to j} = W_{j\to i} = W_{ij}$.

$$W_{ij} = \frac{2\pi}{\hbar^2} \int \left|\left\langle \psi_i \middle| \hat{\mathcal{H}}_1 \middle| \psi_j \right\rangle\right|^2 \rho d\Omega \qquad [3]$$

After stimulation of an ensemble of nuclei with an appropriate $\hat{\mathcal{H}}_1$ by applying a resonant magnetic field $\mathbf{B}_1$ in the form of a radiofrequency (RF) pulse, the measurable signal is the sum of all signals originating from every nucleus in the ensemble. The intensity of the measured signal S_{ij}, corresponding to a transition between energy levels *i* and *j*, is proportional to the combined number of spins N_{ij} in states *i* and *j*, the polarization $P_{ij} = (N_i - N_j)/N_{ij}$ just before the excitation, and the single-nucleus transition probability W_{ij} from Fermi's golden rule, as shown in Equation [4]. The single-nucleus transition probability is proportional to the modulus squared of the matrix element of the perturbative Hamiltonian, $W_{ij} \propto |\langle\psi_i|\hat{\mathcal{H}}_1|\psi_j\rangle|^2$. The signal dependence on the flip angle (FA) arises from this matrix element.

$$S_{ij} \propto N_{ij} P_{ij} W_{ij} \propto (N_i - N_j) \left|\left\langle \psi_i \middle| \hat{\mathcal{H}}_1 \middle| \psi_j \right\rangle\right|^2 \qquad [4]$$

The transition probability formalism suggests that the instantaneous polarization can be obtained directly from measured spectral line intensities. Accurate determination of the proportionality constant can be experimentally difficult, but not necessary if only relative intensities are considered.

Ardenkjaer-Larsen *et al.*, Hurd *et al.*, and Chen *et al.* calculated a spectral parameter known as the C_2 asymmetry, a_{C_2}, defined as the difference of integrals between the lower frequency (upfield, inner) peak and the higher frequency (downfield, outer) peak of the C_2 doublet, all divided by the total C_2 doublet integral, as in Equation [5].

$$a_{C_2} = \frac{S_{C_2}^{(\text{inner})} - S_{C_2}^{(\text{outer})}}{S_{C_2}^{(\text{inner})} + S_{C_2}^{(\text{outer})}} \qquad [5]$$

At thermal equilibrium, $a_{eq} = 0.056$ at 3 T. In literature, the C_1 polarization has been interpreted as $P_{C_1} = a_{C_2} - a_{eq}$. In terms of spin populations, the C_2 asymmetry a_{C_2} can be written as Equation [6] using Equation [4]. It can be seen that the asymmetry $a_{C_2}(t)$ does not correspond directly to the C_1 polarization $P_{C_1}(t)$.

$$a_{C_2}(t) = \frac{[N_1(t) - N_2(t)]\left|\langle\psi_2|\hat{\mathcal{H}}_1|\psi_1\rangle\right|^2 - [N_3(t) - N_4(t)]\left|\langle\psi_4|\hat{\mathcal{H}}_1|\psi_3\rangle\right|^2}{[N_1(t) - N_2(t)]\left|\langle\psi_2|\hat{\mathcal{H}}_1|\psi_1\rangle\right|^2 + [N_3(t) - N_4(t)]\left|\langle\psi_4|\hat{\mathcal{H}}_1|\psi_3\rangle\right|^2} \qquad [6]$$

The theoretical framework supports the correlation between C_1 polarization and C_2 asymmetry, but the relationship is not as simple as $P_{C_1} = a_{C_2} - a_{eq}$. However, we will demonstrate that the C_2 asymmetry, a_{C_2}, correlates strongly with C_1 polarization.

Analogously, the C_1 asymmetry, a_{C_1}, can be defined. In this work, we shall also explore the empirical correlation between C_2 polarization and C_1 asymmetry, a relationship that has not been investigated previously.

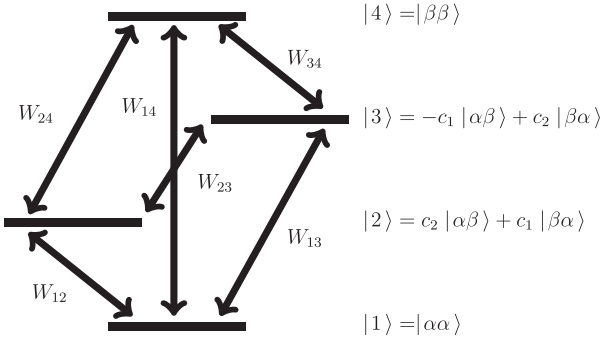

Figure 1. An energy level diagram of a non-weakly *J*-coupled spin-$\frac{1}{2}$ pair. The coefficients c_1 and c_2 represent the degree of superposition of the two mixed uncoupled eigenstates $|\alpha\beta\rangle$ and $|\beta\alpha\rangle$ in the coupled eigenstates $|2\rangle$ and $|3\rangle$. The modulus square of these coefficients represents the probability of measuring a particular eigenvalue in the uncoupled eigenstate basis. The uncoupled eigenstates $|\alpha\alpha\rangle$ and $|\beta\beta\rangle$ remain unchanged as the coupled eigenstates $|1\rangle$ and $|4\rangle$.

METHODS

All experiments were performed using a GE MR750 3 T scanner equipped with 50 mT/m gradients (200 mT/m/ms slew rate) and an 8 kW broadband RF amplifier (GE Healthcare, Waukesha, WI, USA). Animal experiments were approved by the institutional research ethics board and performed in accordance with institutional animal care protocols.

Polarization procedure

Approximately 25 μL of [1,2-$^{13}C_2$] pyruvic acid (99%, Isotec, Miamisburg, OH, USA) doped with 15 mM OX63 trityl radicals (Oxford Instruments, Abingdon, UK) and 1 mM ProHance (Gd-HP-DO3A, Bracco Diagnostics Inc., Princeton, NJ, USA) was polarized to steady state using a HyperSense DNP polarizer (Oxford Instruments). A heated 80 mM NaOH solution with 40 mM NaCl, 40 mM

Tris buffer, and 100 mg/L EDTA was injected in sufficient volume to rapidly dissolve and neutralize the frozen acid. The collection flask was swirled throughout the dissolution process to ensure thorough mixing.

Experiments in blood

Whole blood was extracted from either the femoral or carotid artery of 20 kg pigs into sodium heparin vacuum tubes (BD, Franklin Lakes, NJ, USA) and stored at 4 °C until use. Before the scan, 18 mL of blood was warmed to 37 °C and placed into a 60 mL syringe.

In one experiment, approximately 7 mL of whole blood was extracted from the ear vein of each of three male New Zealand white rabbits and stored in sodium heparin vacuum tubes. Blood type compatibility was verified by mixing 200 μL of blood from each rabbit. The mixture was left for 15 min at room temperature. No clumping was observed after 15 min under ×200 magnification in an optical microscope. To maintain an experimental volume of 18 mL, 6 mL of blood from each rabbit were combined immediately before the experiment. The blood was warmed to 37 °C and placed in a 60 mL syringe.

[1,2-$^{13}C_2$] pyruvic acid was polarized as described above. The hyperpolarized pyruvate solution was transported to the 3 T scanner within 10 s and 2 mL injected through a 92 cm microbore Luer lock-extension set (Codan US Corporation, Santa Ana, CA, USA) into the blood syringe within 20 s. Care was taken to maintain consistent transfer times between repetitions because the evolution of C_2 asymmetry has been observed to depend on the time spent at low field (Keshari K, Wilson D, VanCriekinge M, private communication 2011). A pulse-acquire sequence with 10° FA 200 μs pulses (TR = 3 s, 4096 points/10 kHz readout, 96 transients) was started immediately after injection. A spoiler gradient was played at the end of each TR. Data were acquired with a linear dual-tuned microstrip $^{1}H/^{13}C$ volume rat coil (Magvale, San Francisco, CA, USA).

At thermal equilibrium polarization, 384 transients at 20°C were acquired with 90° FA 200 μs pulses (4096 points/10 kHz readout) after adding 100 μmol Gd-DTPA (200 μL Magnevist, 0.5 mol/L Gd-DTPA, Bayer HealthCare Pharmaceuticals Inc., Wayne, NJ, USA) to shorten the T_1, allowing full magnetization recovery within TR = 10 s. Data from all 384 transients were combined and a 10 Hz Gaussian apodization filter was applied in the time domain. The blood syringe was weighed before and after injection of pyruvate to determine the total amount of [1,2-$^{13}C_2$] pyruvate added to the syringe. Single-transient spectra from a 20 mL [^{13}C] urea phantom (1.0 M ^{13}C with 100 μmol Gd-DTPA) were acquired with 10° and 90° FAs at the end of each experiment. The urea signal intensity and injected weight of pyruvate solution provided an independent quantification of total ^{13}C content in the syringe.

In vivo experiments

A Rowett nude (RNU) rat (Harlan Laboratories, Indianapolis, IN, USA) was anesthetized in an induction chamber under 5% isoflurane with 1 L/min O_2 supply under a protocol approved by the local animal care committee. The rat was transported to the scanner, placed prone into the previously described rat coil, and maintained at 2% isoflurane with 2–3 L/min O_2 supply via a nose cone. Body temperature was maintained at 37.5 °C with a circulating water blanket. A 24 gauge intravenous catheter was inserted into the tail vein. The rat was administered 3 mL of 80 mM pyruvate over 10 s via tail vein injection. A slice-selective pulse with 10° nominal FA was applied every TR = 3 s (4096 points/10 kHz readout, 96 transients) to obtain *in vivo* spectra integrated over a 2 cm slice centred over the rat kidneys.

Data from cardiac metabolic experiments in three pigs were analysed retrospectively in this work. Preparation and handling procedures for pigs have been described previously (7). *In vivo* ^{13}C spectra from pig hearts (integrated over the entire heart) were acquired using a ^{13}C transmit–receive surface coil and a cardiac-gated sequence with nominal 10° hard pulses every 4 R-R beginning simultaneously with intravenous infusion of 15 mL of 83 mM [1,2-$^{13}C_2$] pyruvate over approximately 15 s, as described in (8). The heart rate of each animal was monitored throughout the study and recorded to provide an estimate of TR.

Spectral analysis

Spectral apodization, Fourier transformation, and phasing were performed using SAGE (GE Healthcare). In some experiments, overlap between the two spectral lines of the doublet complicated the partial integral analysis required to obtain $a_{C_2}(t)$ and $a_{C_1}(t)$. Spectral fitting was required to separate the integral contribution from each spectral line. The general shape of each spectral line was approximated using a generalized extreme value probability density function (GEVPDF), which can be written as a function of frequency f in the form of Equation [7]. The GEVPDF was selected because it encompassed a wide range of skewed peak shapes and was easily implementable in MATLAB (MathWorks, Natick, MA, USA). An initial value of $\xi = 0.5$ for the shape parameter and reasonable values for the chemical shift δ_n and width σ_n of each of the n spectral lines were used as initial parameters for the fit.

$$\begin{aligned} y_n(f) &= \frac{1}{\sigma_n} q_n(f)^{\xi+1} e^{-q_n(f)}, \text{where} \\ q_n(f) &= \begin{cases} [1+\xi(f-\delta_n)/\sigma_n)]^{-1/\xi} & \text{if } \xi \neq 0 \\ e^{-(f-\delta_n)/\sigma_n} & \text{if } \xi = 0 \end{cases} \end{aligned} \quad [7]$$

For each of the four pyruvate spectral lines in the phased spectrum, a GEVPDF $y_n(f)$ and a sinc function centred about the chemical shift δ_n were included in the full spectral fitting function $y(f)$, given in Equation [8]. Amplitudes A_n and B_n are positive and w_n denotes the width of the sinc function. The pyruvate hydrate spectral lines were not included in this fit.

$$y(f) = \sum_{n=1}^{4} A_n . y_n(f) - B_n . \text{sinc}[(f-\delta_n)/w_n] \quad [8]$$

In addition to resolving the problem of spectral overlap, this fitting procedure is able to approximate the baseline resulting from the delay between the end of RF excitation and the beginning of data acquisition. This is particularly beneficial in the analysis of spatially localized spectra where the severely rolling baseline is not easily approximated by a polynomial. Better agreement between calculated and experimental baselines was obtained using the fitted baseline as compared with the cubic spline approximation.

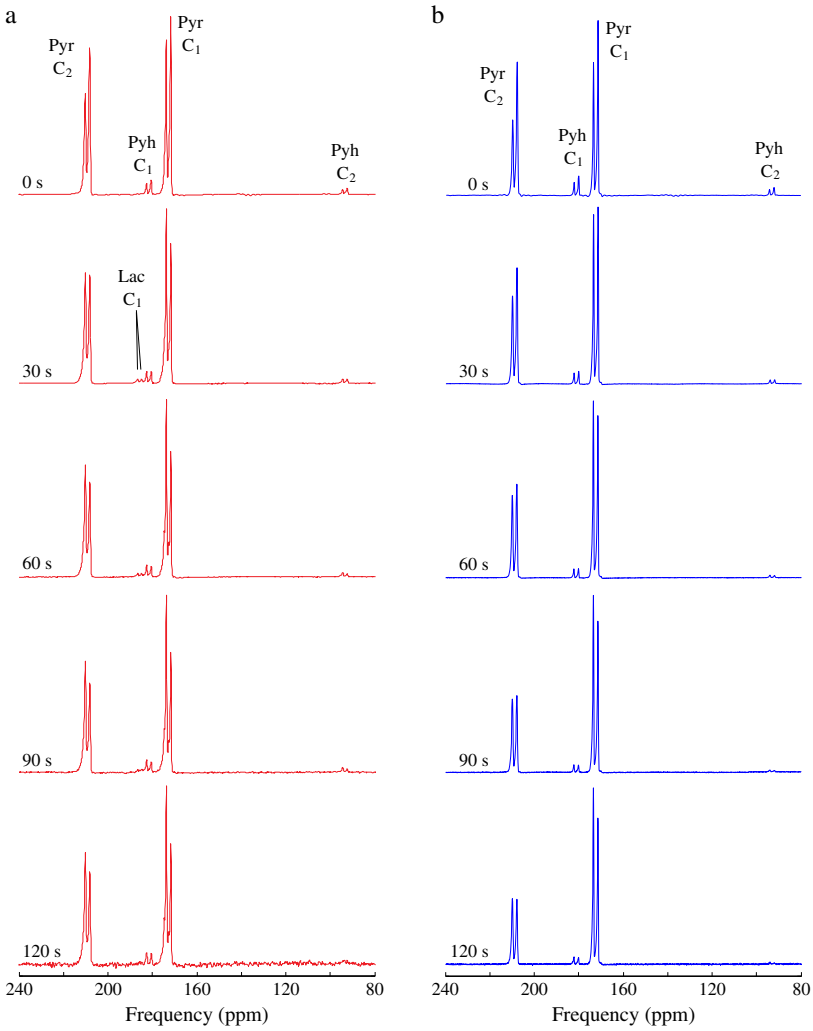

Figure 2. Representative carbon spectra of 80 mM pre-polarized [1,2-$^{13}C_2$] pyruvate (a) injected into 18 mL of 37 °C rabbit blood and (b) in solution at 20 °C. All spectra have been normalized to the same height. Doublets arising from lactate (Lac), the keto form of pyruvate (Pyr), and the gem-diol form of pyruvate (Pyh, pyruvate hydrate) are labelled as shown.

RESULTS

Experiments in blood

Representative *in vitro* carbon spectra of [1,2-$^{13}C_2$] pyruvate injected into rabbit blood are shown in Figure 2(a). Carbon spectra of [1,2-$^{13}C_2$] pyruvate in solution are shown in Figure 2(b) for comparison. The corresponding thermal equilibrium carbon spectra are shown in Figure 3.

Conventionally, the C_1 polarization $P_{C_1}(t)$ for each transient was determined by comparing the C_1 doublet integral to that of the thermal equilibrium spectrum after adjustments for differences in the FA and the number of acquisitions. The analogous analysis was not possible for blood data because a broad resonance centred at 177 ppm, presumably the natural abundance ^{13}C signals of macromolecules in the blood, overlapped with the C_1 doublet and interfered with integration in the thermal equilibrium spectra. As an independent quantification of ^{13}C content in the blood, we prepared a [^{13}C] urea phantom of the same geometry as the blood syringe. The urea signal provides a conversion factor between MR signal intensity and the known amount of ^{13}C in the urea phantom. From the measured mass of injected solution, assuming 80 mM pyruvate concentration in solution, the thermal equilibrium C_1 signal intensity could be estimated using the urea conversion factor for the same gain settings after accounting for FA. For consistency, we report the urea-derived C_1 and C_2 polarizations for all blood experiments.

The asymmetry parameters, a_{C_2} and a_{C_1}, were computed from the fitted spectral line intensities. The correlations between C_1 polarization and C_2 asymmetry for 8 mM [1,2-$^{13}C_2$] pyruvate in whole blood are shown in Figure 4(a) for experiments with 5° FAs ($N = 2$, both pig blood) and in Figure 4(b) for experiments with 10° FAs ($N = 3$, two pig blood and one rabbit blood). The corresponding plots relating C_2 polarization and C_1 asymmetry are shown in Figures 4(c) and 4(d) for experiments with 5° and 10° FAs, respectively.

A linear function with slope m and intercept a_0 was fit to the data; the fitted parameters are summarized in Table 1 according to the data markers in Figure 4. Points with measured polarizations below 1% were not included in the fit because the signal intensity was comparable to the noise levels at these low polarizations. These parameters characterize the mathematical

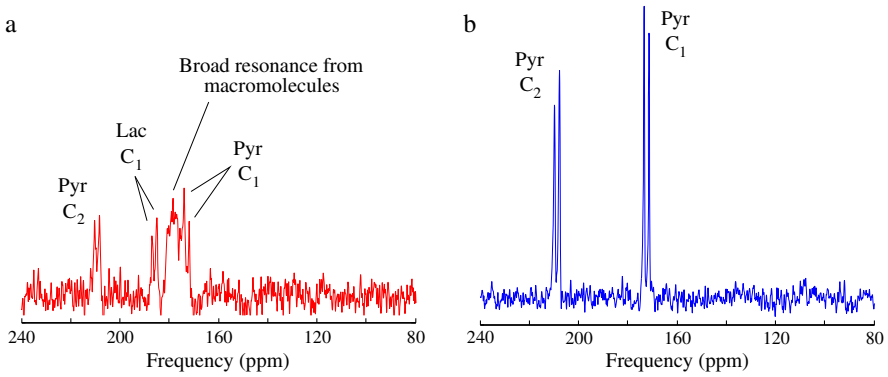

Figure 3. Thermal equilibrium carbon spectra of 80 mM [1,2-$^{13}C_2$] pyruvate (a) in 18 mL of 20 °C rabbit blood doped with 5 mM Gd-DTPA and (b) in solution at 20 °C doped with 4 mM Gd-DTPA. These spectra were formed by combining 384 transients acquired with FA = 90°. Total scan times were (a) 32 min with TR = 5 s and (b) 64 min with TR = 10 s. A 10 Hz Gaussian apodization filter was applied in the time domain before Fourier transform.

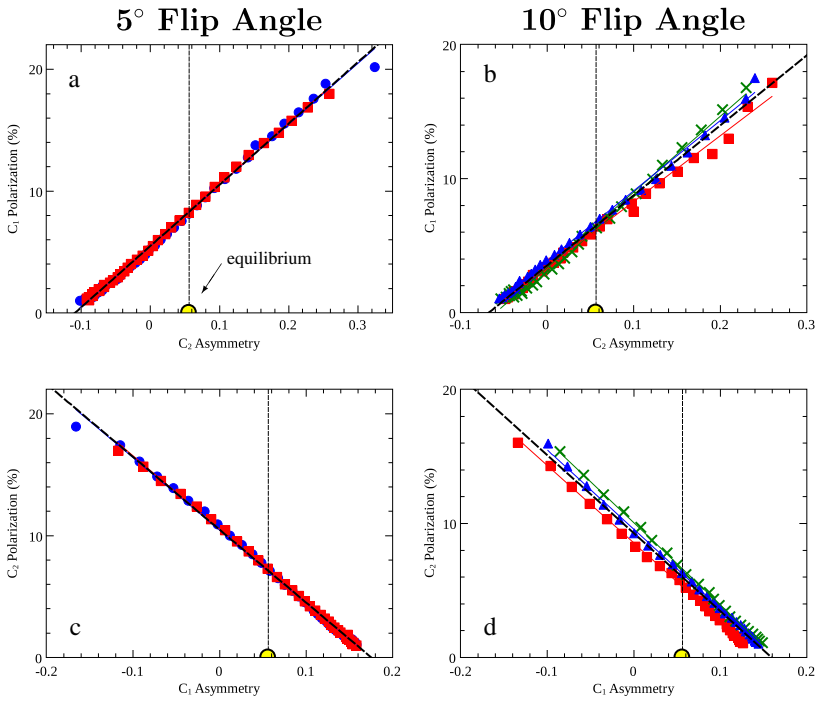

Figure 4. Empirical relationships between doublet asymmetry and polarization in 18 mL of 37°C blood injected with 2 mL of 80 mM pre-polarized pyruvate solution. Panels (a) and (c) show two sets of pig blood data acquired with 5° FAs. Panels (b) and (d) show two sets of pig blood data and one set of rabbit blood data (×) acquired with 10° FAs. A line of best fit is shown for each individual data set. The dashed line shows the best fit to the combined data with computed R^2 values of (a) 0.997, (b) 0.988, (c) 0.997, and (d) 0.981. A highlighted semicircle marks the thermal equilibrium polarization with the thermal equilibrium asymmetry indicated by the connecting dashed vertical line.

models that approximate the experimental data. The curves derived from the average parameters will be considered as calibration curves relating measurable asymmetry to the instantaneous polarization.

A mono-exponential function, with correction for longitudinal magnetization consumption by successive small FA excitations, was fit to the partial integral of each spectral line and to the integral of each doublet, plotted as functions of time, to obtain longitudinal relaxation time constants. These values are summarized in Table 2 according to the data markers in Figure 4. Although the mono-exponential fit modelled the general behaviour of all spectral lines, there was poorer agreement between the downfield partial integrals and the mono-exponential fit ($R^2 < 0.999$), suggesting that the decay may be multi-exponential or non-exponential. Therefore, the values reported in Table 2 may not fully describe the longitudinal relaxation behaviour of some spectral lines. Based on the fit results, the rabbit blood data (×) exhibited shorter longitudinal relaxation time constants compared with the two pig blood data sets with FA = 10°.

In vivo experiments

The average FA = 10° blood calibration curves were used to calculate polarizations from measured doublet asymmetries.

Table 1. Summary of parameters fitted to blood calibration data. Parameters m (%) and a_0 (%) represent the slope and intercept from linear regression. The identifying symbols correspond to the data markers used in Figure 4

		C_2 asymmetry		C_1 asymmetry	
FA	Marker	m (%)	a_0 (%)	m (%)	a_0 (%)
5°	●	50.1	5.49	−59.6	10.45
	■	50.0	5.54	−60.2	10.54
	Average	50.1	5.52	−59.9	10.50
	Std dev.	0.1	0.03	0.4	0.07
10°	×	56.4	3.37	−61.3	10.06
	▲	52.4	3.86	−59.2	9.57
	■	49.0	3.40	−58.0	8.54
	Average	52.6	3.54	−59.5	9.39
	Std dev.	3.7	0.28	1.7	0.78
Average		51.6	4.33	−59.6	9.83
Std dev.		3.0	1.10	1.2	0.82

Table 2. Summary of longitudinal relaxation time constants for spectral lines of 8 mM [1,2-$^{13}C_2$] pyruvate in blood at 37°C. The identifying symbols correspond to the data markers used in Figure 4. All values are given in seconds

		Upfield		Downfield		Doublet	
FA		C_1	C_2	C_1	C_2	C_1	C_2
5°	●	35.6	31.5	48.9	45.8	43.5	37.6
	■	36.2	31.3	47.9	43.5	41.9	35.9
10°	×	27.4	26.6	35.8	36.1	31.7	30.3
	▲	33.0	29.2	44.0	40.9	38.1	33.7
	■	35.4	30.1	47.6	42.1	40.7	34.5
Average		33.5	29.8	45.0	41.8	38.9	34.7
Std dev.		3.7	2.0	5.5	3.7	5.2	2.3

The calculated C_1 and C_2 polarizations are shown in Figure 5(a) as functions of time after the start of injection. Two data points toward the beginning of the acquisition were not included in the analysis because of low SNR.

Estimated *in vivo* T_1 values of 18.6 s (C_1) and 18.8 s (C_2) were obtained by fitting the calculated polarization data to mono-exponential functions, with correction for successive small FA excitations. It is important to note that the relaxation may not be mono-exponential. However, the monotonic decrease in polarization is markedly different from the *in vivo* signal intensity profile shown in Figure 5(b).

Data from a previous study on porcine whole-heart metabolism (8) were reanalysed in this work to investigate the possibility of determining instantaneous polarization from cardiac spectra. The average FA = 10° blood calibration curves were used to analyse these data. The calculated C_1 and C_2 polarizations for three animals are shown in Figure 6(a) as functions of time. It can be seen that a mono-exponential model is not consistent with these data. However, the decreasing trend of the calculated polarization is markedly different from the corresponding signal intensity profile shown in Figure 6(b).

DISCUSSION

A linear function was found to adequately model the calibration data relating instantaneous polarization to doublet asymmetry. The intercept parameter a_0 represents the polarization at which the two spectral lines of the doublet become of equal intensity. Inversion of asymmetry, visually the flipping over of the doublet, occurs for positive values of a_0. It is interesting to observe that $a_{eq} \neq -a_0/m$, which suggests that this model does not completely describe the relaxation back to thermal equilibrium. The spectral behaviour in the latter stages of relaxation back to thermal equilibrium remains a mystery because the signal intensity at polarizations below 1% becomes comparable to the level of noise under the described experimental conditions. However, we have shown that the linear model provides an adequate estimation of calibration data over the range of usable SNR, approximately 1 min *in vivo*.

[1-^{13}C] pyruvate is expected to have a slightly longer T_1 than [1,2-$^{13}C_2$] pyruvate *in vivo*. However, the low C_2 SNR from the 1% natural abundance of [1,2-$^{13}C_2$] pyruvate in [1-^{13}C] pyruvate limits polarization measurement to a small number of time points. To increase the C_2 SNR, we propose the co-polarization of [1-^{13}C] pyruvic acid with a small amount, e.g. 5%, of [1,2-$^{13}C_2$] pyruvic acid. The longer T_1 of the predominantly singly

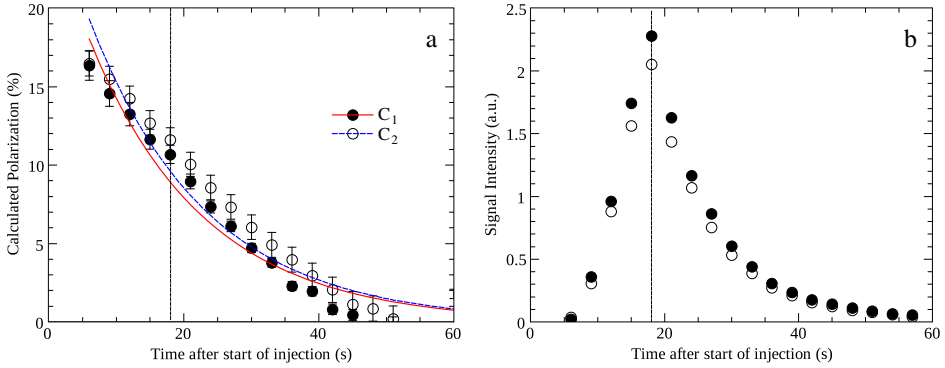

Figure 5. (a) The decay of *in vivo* C_1 (closed symbols) and C_2 (open symbols) polarization observed in the rat kidneys calculated using the average FA = 10° blood calibration curves. The error bars show the propagated errors representing the statistical uncertainties in the calibration curve parameters. Exponential curves of best fit, with FA correction, are shown for the decay of C_1 (solid curve) and C_2 (dashed curve) polarization. (b) The corresponding signal intensity profiles for C_1 (closed symbols) and C_2 (open symbols) doublets, in arbitrary units, as functions of time. The dashed vertical line marks the time of maximal signal intensity on both panels.

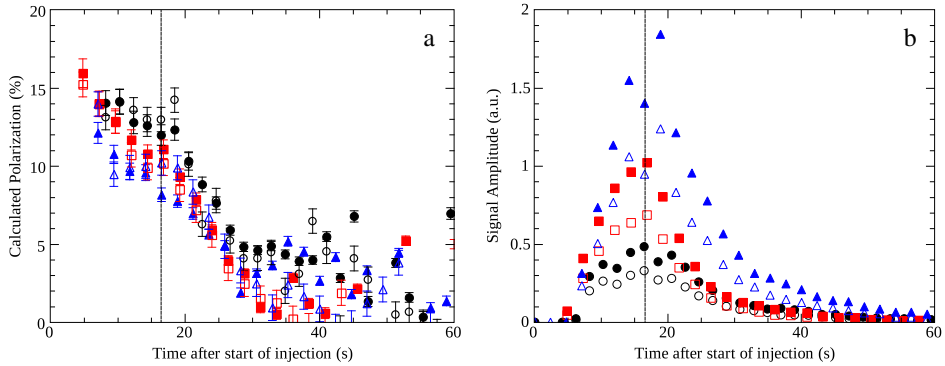

Figure 6. (a) Estimated *in vivo* C_1 (closed symbols) and C2 (open symbols) polarization decay in three experiments observing the whole pig heart. The error bars show the corresponding propagated errors representing the statistical uncertainties in the calibration curve parameters. (b) The corresponding signal intensity profiles for C_1 (closed symbols) and C_2 (open symbols) doublets as functions of time. The dashed vertical line marks the time of maximal signal intensity on both panels.

labelled pyruvate may prolong the available imaging time using the C_1 signal, while the enhanced C_2 signal in the spiked mixture may facilitate the monitoring of C_1 polarization at a greater number of time points throughout the imaging, assuming similar polarizations are achieved for [1-^{13}C] pyruvic acid and [1,2-$^{13}C_2$] pyruvic acid.

Unequal relaxation rates of the two lines within a doublet is a common observation in the presence of cross-correlations in a strongly coupled two-spin system, a phenomenon known as "the multiplet effect" (9). In addition to auto-correlated dipolar relaxation between C_1 and C_2, contributions from cross-correlated relaxation mechanisms (10) may result in non-exponential relaxation, which may further influence the evolution of the doublet asymmetries in [1,2-$^{13}C_2$] pyruvate. The values in Table 2 are reported as longitudinal relaxation time constants (τ) because T_1 may not be defined in cases of non-exponential relaxation.

Although density matrix simulation provided accurate predictions of C_2 asymmetry over a short period after placement in the scanner, agreement between simulation and measurement gradually worsened as the two-spin system was allowed to evolve at field (6). Inclusion of cross-relaxation effects in the simulation may improve its predictive accuracy. However, even for the simple system of [^{13}C] formate, monitoring of ^{13}C polarization using the ^{1}H doublet asymmetry required careful modelling of the $^1H - {}^{13}C$ dipolar cross-relaxation in solution (11). In blood, endogenous molecules may introduce additional relaxation pathways that could further complicate the modelling. Whereas a separate theoretical model would be required for each medium of interest (e.g. serum, normal saline, gels), the protocol described in this work can be applied with little modification to obtain calibration data in arbitrary media.

We have demonstrated that the relationship between C_1 polarization and C_2 asymmetry is much richer than $P_{C_1} = a_{C_2} - a_{eq}$, as previously reported in literature. In particular, we have shown that $m < 100\%$ and $a_0 \neq -a_{eq}$ for the conditions that we examined. The empirical interpretation of asymmetry ensures that unphysical negative polarizations of the coupled carbon are not predicted when the doublet evolves beyond the asymmetry at thermal equilibrium. Furthermore, relating asymmetry to polarization of the coupled carbon via empirical calibration is relatively straightforward and potentially more robust compared with some theoretical approaches. For example, longitudinal relaxation is known to be field dependent. Slower longitudinal relaxation at low field (< 0.1 T) has been exploited to reduce the loss of polarization of [1-^{13}C] pyruvate before placement into the high field of the scanner (12). The effects of slower relaxation at low field on the evolution of pyruvate doublet asymmetries are not well understood, but the calibration-based approach naturally takes into account any evolution that occurs at low field (assuming consistent transfer times between calibration and *in vivo* experiments) without the need to actively correct for the complex spin dynamics that occur during transport from polarizer to scanner.

From density matrix simulations, the asymmetry in the spectral intensities of the C_2 doublet was identified as originating from the two-spin order term of the density matrix (13). We have demonstrated, in blood, an FA dependence in the calibration parameters, which was consistent with simulation and theoretically expected because the line intensities of an AB system depend on the FA if the spin system is not in thermal equilibrium immediately prior to RF pulse application (14). The FA dependence in the calibration parameters may pose some limitations on the choice of pulse sequences. One important case that Tropp considered was the disappearance of spectral asymmetry after the application of a 90° pulse due to complete conversion of two-spin order into double and zero quantum coherences. Pulse sequences with spectrally non-selective 90° pulses may not be compatible with this polarization quantification technique. However, the use of spectrally selective pulses, which excite only one of the two nuclei at a time, may allow interleaved imaging and polarization measurement.

One potential concern regarding the usefulness of this calibration-based technique may be the inter-patient applicability of calibration data. For FA = 5°, calibration data obtained using blood from two different animals are shown in Figures 4 (a) and 4(c). Agreement between the two data sets was better than 1%, which suggests good tolerance for blood chemistry variability between patients. The large deviation of the first data point in each series from the fitted trend may be attributed to incomplete mixing immediately after the injection. Factors such as haematocrit and blood oxygenation were not examined in detail in this study. Further investigation is required to determine the limits of inter-patient variability.

Another concern may be the validity of using non-human blood results to suggest the potential suitability of this calibration technique for human use. A comparison between the two pig blood calibration curves (■ and ▲) and the rabbit blood calibration curve (×) in Figures 4(b) and 4(d) shows that any one of the curves predicts polarization values within ±1% of the other curves over the range of asymmetries observed. Furthermore, there was close agreement among the three curves even though the longitudinal relaxation time constants in rabbit blood were shorter than those in pig blood, which may be consistent with signal transfer from pyruvate to its downstream metabolites due to higher erythrocyte metabolic activity in rabbit blood. One advantage of using doublet asymmetries instead of signal intensities for polarization measurement is the concentration-insensitivity of the asymmetry parameters, a_{C_1} and a_{C_2}, which are normalized for signal intensity by definition. Polarizations that are derived from doublet asymmetry are largely unaffected by metabolic activity unless the rate of label exchange in both directions may become comparable, as in the case of pyruvate–lactate co-injections with both substrates labelled (15).

In vivo C_1 and C_2 longitudinal relaxation time constants of 19 s were estimated by fitting the rat kidney polarization decay curves to mono-exponential functions. Although the relaxation may not be truly mono-exponential, we observe that a mono-exponential fit approximately models the dominant relaxation behaviour. Both C_1 and C_2 polarizations decreased monotonically with time, which differ markedly from the time profiles of signal intensity. The calculated C_2 polarizations were slightly higher than the calculated C_1 polarizations, but there was no significant difference within statistical uncertainty. However, the agreement (within uncertainty) between the C_1 and C_2 longitudinal relaxation time constants is consistent with the *in vitro* longitudinal relaxation behaviour in blood.

Unlike the rat kidney data, the calculated C_1 and C_2 polarization decay curves in pig hearts are evidently non-exponential. An overall monotonically decreasing trend can be seen with increasing fluctuation in the data. Blood in the different chambers of the heart may have experienced different relaxation histories such that the doublet asymmetries are different in the various compartments. By integrating the signal over the whole heart, only the averaged doublet asymmetry was observed. However, the average doublet asymmetry may not reflect the relaxation behaviour of any compartment. The blood calibration data may not be valid under such circumstances, resulting in a nonsensical analysis. It may be worthwhile to investigate the feasibility of polarization measurement in localized cardiac spectral data that distinguish between the different compartments of the heart.

It is important to recognize that relaxation conditions in tissue may differ from those in blood. Although it can be argued that blood calibration data provide a good model for examining experimental data in the vasculature, the validity of using blood calibration data to analyse spectra localized to regions where tissue content dominates may be less convincing. To ensure validity of the calibration data, it is suggested that localized spectra intended for polarization measurement be acquired in the vasculature immediately upstream of the tissue of interest. The measured polarization should provide a good estimate for the initial polarization in the tissue of interest. Further investigation is required to characterize the errors that could arise from using blood calibration data to analyse spectra localized to tissue-dominated volumes.

CONCLUSIONS

In this work, we have presented a calibration-based method for real-time measurement of pyruvate polarization that can be used for *in vivo* applications. The calibration data offered some new insights into the framework of J_{CC} spectral asymmetry previously established in literature. One important observation in blood is that the C_2 asymmetry is linearly related to the C_1 polarization with a slope that is less than unity. The empirical interpretation of C_2 asymmetry ensures that unphysical negative C_1 polarizations are not predicted when the C_2 doublet evolves beyond the asymmetry at thermal equilibrium. Furthermore, we have demonstrated the feasibility of measuring *in vivo* C_2 polarization using the C_1 doublet asymmetry.

The approach we have presented offers great flexibility and is suitable for a variety of experimental protocols. The collection of empirical calibration data naturally accounts for differences in the medium of interest and transfer times between polarizer and scanner, which may be difficult to model theoretically. Preliminary data suggest good inter-patient applicability. This novel interpretation of spectral asymmetry extends its predictive value to the full range of usable SNR. The *in vivo* polarization decay curves obtained using this technique allow us to report, for the first time, the *in vivo* T_1 of pyruvate C_1 and C_2.

Despite the robustness of this method, care must be taken in acquiring calibration data such that all environmental conditions are similar to those used in experimental protocols. *In vivo* polarizations extracted from asymmetry in the vasculature, immediately upstream of the tissue of interest, are expected to be much closer estimates of the polarization in tissue compared with polarization measurements from previously established techniques.

Acknowledgements

The authors thank Jennifer Barry, Michelle Ladouceur-Wodzak, and Carrie Purcell for their assistance with animal experiments. Funding support was provided by the Ontario Institute for Cancer Research, the Natural Sciences and Engineering Research Council of Canada, and the Ontario Graduate Scholarships program.

REFERENCES

1. Ardenkjaer-Larsen JH, Fridlund B, Gram A, Hansson G, Hansson L, Lerche MH, Servin R, Thaning M, Golman K. Increase in signal-to-noise ratio of >10,000 times in liquid-state NMR. Proc. Natl. Acad. Sci. 2003; 100(18): 10158–10163.
2. Kohler SJ, Yen Y, Wolber J, Chen AP, Albers MJ, Bok R, Zhang V, Tropp J, Nelson S, Vigneron DB, Kurhanewicz J, Hurd RE. *In vivo* ^{13}carbon metabolic imaging at 3T with hyperpolarized ^{13}C-1-pyruvate. Magn. Reson. Med. 2007; 58(1): 65–69.
3. Golman K, in't Zandt R, Lerche M, Pehrson R, Ardenkjaer-Larsen JH. Metabolic imaging by hyperpolarized ^{13}C magnetic resonance imaging for *in vivo* tumor diagnosis. Cancer Res. 2006; 66(22): 10855–10860.
4. Schroeder MA, Clarke K, Neubauer S, Tyler DJ. Hyperpolarized magnetic resonance: a novel technique for the *in vivo* assessment of cardiovascular disease. Circulation 2011; 124(14): 1580–1594.
5. Hurd RE, Chen A, Cunningham CH, Tropp J. Scalar coupling patterns in hyperpolarized spin systems: J_{CC} spectral pattern in hyperpolarized 1,2-[^{13}C]-pyruvate. A potential indirect measure of polarization. *Proceedings of the 50th Experimental Nuclear Magnetic Resonance Conference*. Pacific Grove, CA, 2009, p. 438.
6. Chen AP, Cunningham CH, Tropp J, Keshari K, VanCriekinge M, Kurhanewicz J, Hurd RE. Potential for polarization measurement of

pre-polarized [1-^{13}C] pyruvate *in vivo* using Jcc spectral pattern. *Proceedings of the International Society of Magnetic Resonance in Medicine*, volume 18. Stockholm, 2010, p. 3261.
7. Lau AZ, Chen AP, Hurd RE, Cunningham CH. Spectral–spatial excitation for rapid imaging of DNP compounds. NMR Biomed. 2011; 24(8): 988–996.
8. Chen AP, Hurd RE, Schroeder MA, Lau AZ, Gu Y-P, Lam WW, Barry J, Tropp J, Cunningham CH. Simultaneous investigation of cardiac pyruvate dehydrogenase flux, Krebs cycle metabolism and pH, using hyperpolarized [1,2-$^{13}C_2$]pyruvate *in vivo*. NMR Biomed. 2012; 25(2): 305–311.
9. Campbell ID, Freeman R. Influence of cross-relaxation on NMR spin-lattice relaxation times. J. Magn. Reson. 1973; 11(2):143–162.
10. Kumar A, Grace RCR, Madhu PK. Cross-correlations in NMR. Prog. Nucl. Magn. Reson. Spectrosc. 2000; 37(3): 191–319.
11. Merritt ME, Harrison C, Mander W, Malloy CR, Sherry AD. Dipolar cross-relaxation modulates signal amplitudes in the ^{1}H NMR spectrum of hyperpolarized [^{13}C]formate. J. Magn. Reson. 2007; 189(2): 280–285.
12. Van Criekinge M, Keshari K, Wilson DM, Vigneron DB, Kurhanewicz J. Retaining polarization by exploiting slower T_1 relaxation of hyperpolarized spins at low field in solution. *Proceedings of the 53rd Experimental Nuclear Magnetic Resonance Conference*. Miami, FL, 2012, p. 139.
13. Tropp J. Multiplet asymmetry and multi-spin order in liquid-state NMR spectra of hyperpolarized compounds. *Proceedings of the International Society of Magnetic Resonance in Medicine*, volume 18. Stockholm, 2010, p. 1026.
14. Bain AD, Martin JS. FT NMR of nonequilibrium states of complex spin systems. I. A Lionville space description. J. Magn. Reson. 1978; 29(1): 125–135.
15. Park JM, Hurd RE, Josan S, Yen Y-F, Pfefferbaum A, Mayer D, Spielman DM. Differentiation of flux and isotopic exchange using co-administration of hyperpolarized [2-13C]Pyr and [1-13C]Lac. *Proceedings of the International Society of Magnetic Resonance in Medicine*, volume 20. Melbourne, 2012, p. 4298.